Light-Controllable Electroconvection Patterns in a Chiral Nematic Liquid Crystal

Hongzhen Jing,[1] Ying Xiang,[1,*] Mingya Xu,[1] Everett Wang,[1] Jing Wang,[1] Nándor Éber,[2] and Ágnes Buka[2]

[1]*School of Information Engineering, Guangdong University of Technology, Guangzhou 510006, P. R. China*
[2]*Institute for Solid State Physics and Optics, Wigner Research Centre for Physics, Hungarian Academy of Sciences, H-1121 Budapest, Konkoly-Thege Miklós út 29-33, Hungary*

(Received 18 January 2018; revised manuscript received 20 May 2018; published 27 July 2018)

The influence of UV light-induced pitch contraction and dilation on the electroconvection patterns (ECPs) of a chiral nematic liquid crystal containing a photoresponsive chiral dopant is investigated in planar-aligned cells. It is observed that the helical twisting power of the dopant changes (even undergoes handedness inversion) under UV irradiation; consequently, the pitch and the direction of the convection rolls in ECPs (being either parallel with or perpendicular to the surface alignment) could be controlled by the UV intensity and the ac voltage. In contrast to traditional methods, where the pitch is modulated by electric or thermal fields, our method of applying a light field allows a remote and contactless manipulation of the pitch, which is easily detectable via the morphological changes of ECPs. The ability to control the orientation of ECPs by tuning the light intensity can conveniently be utilized as an optical grating, allowing switchable, dual-mode operation.

DOI: 10.1103/PhysRevApplied.10.014028

I. INTRODUCTION

Nematic liquid crystals (NLCs) are fluids, whose molecules self-assemble into a mesophase possessing long-range orientation order characterized by a director **n** [1]. Due to their inherent anisotropies, the equilibrium director field of NLCs can easily be perturbed by an external (e.g., electric) field. When subjected to inhomogeneous or even to homogeneous fields, this perturbation often may take the form of extended, regular structures (patterns); their morphology can be tuned by the parameters of the fields. The periodicity of these patterns can be in the micrometer range and comparable with the optical wavelengths. Thus, they may serve as optical gratings, and investigations on the formation of such microstructures have attracted considerable interest in the field of optics [2–5].

One particularly interesting structure is the electroconvection pattern (ECP) [6–9]. Planar-aligned NLCs with non-negligible electrical conductivity, negative dielectric, and positive conductivity anisotropies ($\Delta\epsilon < 0$ and $\Delta\sigma > 0$) often exhibit electroconvection (EC). ECPs emerge if the applied ac voltage exceeds a threshold value $U_{\rm th}$; the instability arises due to the couplings among the orientation of the director, the flow of both material and charge, and the electric field. There is a frequency range of the applied ac voltage, where EC is manifested in the appearance of normal rolls (Williams domains), characterized by stripes with a periodicity of $\Lambda \approx 1$–$2\ d$ (d is the thickness of the LC layer), running perpendicular to the initial director $\mathbf{n}_0$ that is determined by the surface orientation [6–9]. Formation of such normal rolls can be explained via the Carr-Helfrich feedback mechanism [10]: a periodic fluctuation in the director tilt leads to space-charge separation due to the anisotropic conductivity; the Coulomb force on the space charges induces a vortex flow, which exerts a destabilizing torque on the director. This feedback becomes positive at voltages above $U_{\rm th}$; thus the fluctuations may grow to a macroscopic ECP.

The aforementioned EC phenomenon also exists in chiral nematic (cholesteric) liquid crystals (CLCs), though it becomes more intriguing and diversified. CLCs can conveniently be induced by adding chiral dopants to an NLC. The equilibrium state of the resultant CLCs is a helical director field characterized by a helical pitch P_0, which depends on the concentration C and the helical twisting power (HTP) β of the chiral dopant. For low-dopant concentrations one expects $P_0 = (C\,\beta)^{-1}$ [1].

As one might expect, the presence of a helical structure has noteworthy consequences on the threshold behavior (the threshold voltage and the morphology at onset) of ECPs. Pioneering experiments proved that the standard ECP types of nematics (the conductive and the dielectric rolls) are observable in CLCs as well [11–15]. In addition, square grid patterns were also reported [13–17]. Typically, roll patterns occurred in long-pitch CLCs, while grids were detected in short-pitch CLCs. The first theoretical model

*frank_xiang68@qq.com

of this pattern formation by Helfrich and Hurault [18–20] predicted a threshold voltage $U_{th} \propto (d/P_0)^{1/2}$. Experimental results on planar-aligned CLCs, however, did not match this prediction; they rather exhibited a nonmonotonic dependence of the threshold on the sample thickness [21–26]. This discrepancy was attributed to the fact that planar CLCs possess a Grandjean texture [1]. Strong anchoring at the bounding surfaces requires the presence of an integer number (k) of the helical half turns of the director ($d = k\ P/2$). The constrained pitch P may differ from the equilibrium pitch value P_0 of the bulk sample at the prevailing conditions. Measurements indicated an increase of the threshold voltage for compressed helices and reduced U_{th} for dilated helices. These observations were justified by calculations based on the continuum theory [23–25,27]. Careful experimental and theoretical studies of the thickness dependence in the small k (<3) range using a wedge-shaped cell uncovered that besides U_{th}, the wave vector of the rolls is also affected by the number of helical half turns: rolls normal to the surface director $\mathbf{n}_0$ are present for $k = 0$ and $k = 2$, but rolls parallel with $\mathbf{n}_0$ are formed for $k = 1$ [22,23].

In view of the findings above, we conclude that the helical structure is the key factor to determine the multifariousness of pattern morphologies in CLC systems. Controlling the helical structure by specific external actions is, therefore, a highly desirable, though challenging work [28–31]. Thorough investigations were performed by altering the concentration of dopants [15], the surface alignments [32], the temperature [33,34], and the strength of the ac field [35]; even some ionic liquids have been tested, in which chirality can arise from either the anion, or the cation, or both [36].

Recently, these efforts were extended to include light stimulus:

(i) Some studies focused on the photoisomerization effect of azo groups, whose *trans-cis* conformation change reoriented the host CLC molecules via intermolecular coupling, resulting in a change of the helical pitch. Thus photoirradiation of the CLCs containing azo dyes gave rise to optical switching between different electro-optic modes [37–39]. For example, a waveband-selective diffraction grating, allowing dynamic and reversible light manipulation, was developed by micropatterning CLCs doped with an azo dye [40]. The diffraction resulted from the periodic amplitude modulation (alternating transmittance and reflectance of light) between exposed and unexposed CLC areas, in contrast to the traditional phase modulation in CLC gratings [41].

(ii) Other works were based on photoresponsive chiral dopants, whose helical twisting power and thus the induced helical structure could be tuned, depending on the material properties, the surface conditions and the field parameters. For example, an optical intensity-driven self-organized helical superstructure in one-dimension (1D) was observed to exhibit a wide bandgap with reversible dynamic shifting, where the change of the helical pitch and even a chiral handedness inversion were obtained upon UV exposure [42]. This 1D work was extended to rotate the helical axis in the 3D space [43,44]. As another example, structural changes in CLCs caused by the optically induced helix inversion in a homeotropic cell were observed [45], including a sequence of structural transformations from the "lying left-handed helix" through an "unwound homeotropic state" to the "lying right-handed helix." Afterwards, an optically rotatable phase grating of CLCs in a hybrid cell was proposed. Due to the nonphotochromic and photosensitive chiral dopants, the helix handedness of CLCs could be photo-switched reversibly. It was shown that the irradiation by UV light rotates the diffraction gratings clockwise, whereas the irradiation by visible light induces a counterclockwise rotation [46].

Investigation of ECPs and exploration of the underlying mechanisms will lead to a better understanding of the physical behavior of LCs; thus facilitating applications. For example, ECPs have been exploited as controllable optical gratings to modulate light [47], which is of interest in optical-information processing. Current efforts mainly focus on the exploration of ECPs driven by an electric field only [48,49]. A comprehensive study of ECPs driven by combined electric and light fields has not yet been carried out.

Herein, we use a photoresponsive chiral dopant to explore the EC phenomena in CLC systems, where upon UV light, ECPs with different morphologies and threshold voltages can be induced and switched. Furthermore, we clarify that the change of the pitch P is responsible for the transformation of ECPs; thus we can readily control the morphologies of ECPs by UV light.

The optical tuning of ECPs in CLCs has distinct advantages in academic research as well as in practical applications. For example, it can be used as an alternative method to explore the origin of the EC effect and clarify the influence of the helical structure on the formation of ECPs. This enables us to gain deeper insights into the fundamental understanding on how LC molecules, electric and light fields interplay with each other, as well as how the induced complex structures form. Such information can be further used as a guideline to develop alternative photonic devices, taking advantage of the easy, instant, precise, and remote tunability of light. For example, traditional ECPs are periodic usually only in one dimension (x direction), whereas in our case, ECPs can be switched between orthogonal directions (x and y directions) with light. Thus optical gratings based on our ECPs can implement dual-mode operations switched *in situ* by light field.

II. MATERIAL AND EXPERIMENTAL ARRANGEMENT

The CLC materials used here are composed of the host NLC 4-*n*-octyloxyphenyl 4-*n*-methyloxybenzoate (1OO8) [50] doped with the initially left-handed chiral dopant 9-(2-methyl-2,3-dihydro-1H-cyclopenta[a]naphthalen-1-ylidene)-9H-fluorene (M5). M5 is the left-handed isomer from the racemic saturated alkene after chiral resolution by high-performance liquid chromatography (HPLC), while M1 in Ref. [42] is the right-handed one.

The phase transition temperatures of CLCs depend on the nematic range of the host 1OO8 (between 53 and 76.7 °C), and on the weight concentration (C_{M5}) of the dopant M5. For example, at $C_{M5} = 1.2\%$ that is used as the primary composition in the following, the chiral nematic phase is present between 23 and 61 °C.

The experimental setup used for the measurements is sketched in Fig. 1.

For all measurements reported in Sec. IV, the CLC materials are filled into standard, $d = 6$-μm-thick planar cells of 16 $\times$ 8 mm^2 size. The two ITO glass substrates are coated with polyimide and antiparallel rubbing of those substrates ensures that the orientation of CLC molecules on the surface are planar, along $\mathbf{n}_0$. This alignment technique resulted in typical uniform planar textures, indicating that the helical axis is perpendicular to the substrates. The temperature of the samples is kept constant at $T = 40$ °C by using a Linkam LTS 350 heating stage with a TMS 94 temperature controller.

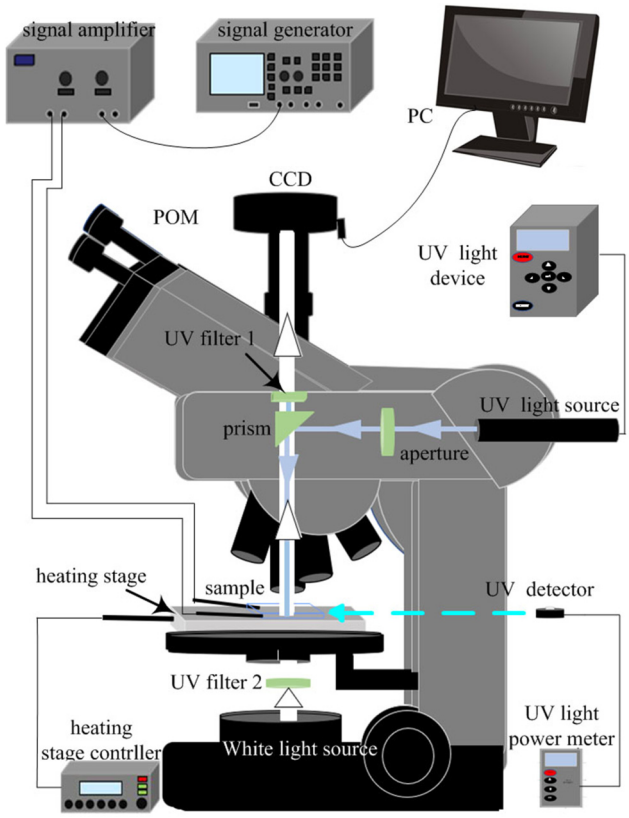

FIG. 1. Sketch of the experimental setup.

A sinusoidal ac voltage of rms value U is applied to the samples through an amplifier. The resulting electric field is perpendicular to the substrates and $\mathbf{n}_0$. The induced ECPs are observed by a polarizing microscope (POM) equipped with a high-resolution CCD camera, in transmission mode at crossed polarizers (analyzer $\mathbf{A} \perp$ polarizer $\mathbf{P}$) using a white light source. For UV irradiation of the CLC samples a UV LED source (FUV-8BIT, Height-LED Optoelectronics Technology Co.) is used; its light is coupled into the microscope in reflection mode through a prism (Fig. 1). A UV filter is positioned above the prism to protect the camera, and another UV filter blocked any accidental UV content of the white light source from reaching the sample. The UV intensity is measured by a UV-B dual-channel irradiation meter positioned on the top surface of the sample.

III. CHARACTERIZATION OF THE PITCH

In general, the natural pitch P_0 of an induced CLC is determined by the concentration C and the helical twisting power β of the chiral dopant; the latter is usually temperature dependent. For low dopant concentration, one expects $P_0 = (\beta\ C)^{-1}$ [1].

Our dopant M5 is, however, a photoresponsive dye behaving like a molecular motor. When subjected to UV exposure, it undergoes photoisomerization. Its rotor part rotates with respect to the stator part around the carbon double bond, from the stable form M5(P) in Fig. 2(a) to an unstable form M5(M) in Fig. 2(b). After switching off the UV light, the dopant recovers its stable M5(P) form through thermal relaxation. The unstable M5(M) conformer has an opposite handedness compared to the stable M5(P) conformer; hence their HTP values, β_P and $\beta_M \approx -\beta_P$, are different. The photoisomerization also affects the absorption spectrum of the dopant. Figure 2(c) depicts the absorption at different UV intensities. It can be noticed that when increasing the UV intensity, the absorption reduces in the UV range at the expense of that at the visible wavelengths.

Due to the photosensitivity of the M5 dopant, in the presence of UV irradiation, both conformers are present in the system. Their concentrations, $C_P(I)$ and $C_M(I)$, depend on the UV intensity I and are subjected to the constraint that the total dopant concentration,

$$C_{M5} = C_P(I) + C_M(I), \tag{1}$$

is fixed. The CLCs thus behave as a nematic host doped with two dopant species, M5(P) and M5(M), both having UV-intensity-dependent concentrations. Then the natural

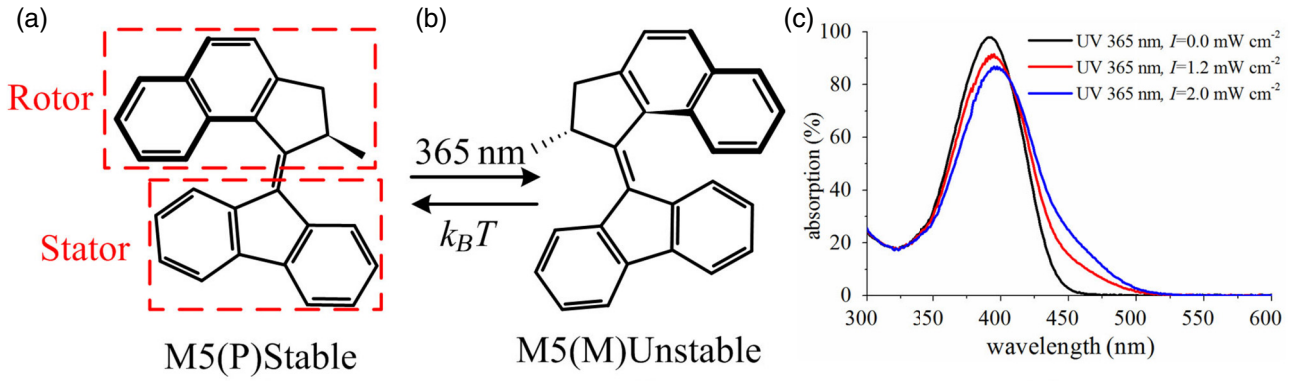

FIG. 2. (a) Molecular structure of the chiral dopant M5 in dark. (b) Molecular structure of M5 after photoisomerization (k_B is the Boltzmann constant and T is the absolute temperature). (c) UV-visible absorption spectra of the M5 solution in CH_2Cl_2 (20 μg/ml) under illumination by different UV intensities.

helical pitch $P_0(I)$ also depends on the UV intensity:

$$P_0(I) = [\beta_M C_M(I) + \beta_P C_P(I)]^{-1}. \tag{2}$$

In view of the constraint in Eq. (1), we introduce a UV-intensity-dependent effective HTP, $\beta_{\mathrm{M5}}(I)$, for the illuminated dopant M5 via the relation

$$P_0(I) = [\beta_{\mathrm{M5}}(I) C_{\mathrm{M5}}]^{-1}. \tag{3}$$

The intensity dependence of this effective HTP can be estimated via the following simple model. First we assume, that in equilibrium in dark, only the stable conformer M5(P) is present. Under irradiation by UV intensity I, some stable conformers are excited into the unstable state M5(M), but besides the simple thermal relaxation some unstable conformers are also forced to return to the stable state. Thus the relative concentration $X = C_M(I)/C_{\mathrm{M5}}$ of the unstable conformer is governed by the rate equation [51]

$$\frac{dX}{dt} = \kappa_{PM} I(1 - X) - \kappa_{MP} I X - \frac{X}{\tau}, \tag{4}$$

where κ_{PM} and κ_{MP} are the rates of the UV-induced M5(P) $\rightarrow$ M5(M) and M5(M) $\rightarrow$ M5(P) transformations, respectively, while τ^{-1} is the rate of the thermal relaxation.

In equilibrium, when the time derivative vanishes, $x(I)$ can be expressed with a saturation concentration X_s at $I \rightarrow \infty$ and a scaling intensity I_0 as

$$X(I) = X_s \frac{I}{I + I_0}, \quad \text{with } X_s = \frac{\kappa_{PM}}{\kappa_{PM} + \kappa_{MP}} \leq 1 \quad \text{and}$$
$$I_0 = \frac{1}{(\kappa_{PM} + \kappa_{MP})\tau}. \tag{5}$$

Then, combining Eqs. (2) and (3) one obtains

$$\beta_{\mathrm{M5}}(I) = \beta_P \left[1 - \left(1 - \frac{\beta_M}{\beta_P}\right) X(I)\right]. \tag{6}$$

As the HTPs of the two conformers are of opposite sign, there is a critical UV intensity I_c,

$$I_c = I_0 \frac{1}{[1 - (\beta_M/\beta_P)]X_s - 1}, \tag{7}$$

where the helix becomes compensated [unwound, $|P_0(I_c)| = \infty$, $\beta_{\mathrm{M5}}(I_c) = 0$]. Passing I_c with the intensity a handedness inversion occurs. Combining Eqs. (6) and (7) yields

$$\beta_{\mathrm{M5}}(I) = \beta_P \left[1 - \frac{I_c + I_0}{I_c} \frac{I}{I + I_0}\right], \tag{8}$$

i.e., the effective HTP depends only on I_0 and I_c.

As already mentioned in Sec. I, due to the strong planar surface anchoring, in planar-aligned CLC samples the number k of the helical half turns of the director across the CLC layer must be an integer (Grandjean texture) [1]. Consequently, the actual pitch $P = 2\,d/k$ is determined by the sample thickness d and thus typically does not coincide with P_0. For $|P| < |P_0|$, the cholesteric helix becomes contracted, while for $|P| > |P_0|$ it is dilated. For a given thickness, k is singled out as the integer that minimizes the elastic free energy

$$F(k) = \frac{1}{2} K_2 \left(\frac{k\pi}{d} - \frac{2\pi}{P_0}\right)^2 \tag{9}$$

of the sample (K_2 is the twist elastic modulus). After simple calculations the relations $F(k) \leq F(k-1)$ and $F(k) \leq F(k+1)$ yield the inequalities

$$\frac{2d}{P_0} - \frac{1}{2} \leq k \leq \frac{2d}{P_0} + \frac{1}{2}, \tag{10}$$

which provide the pitch limits for a sample with k half turns. These facts will play an important role in further discussions.

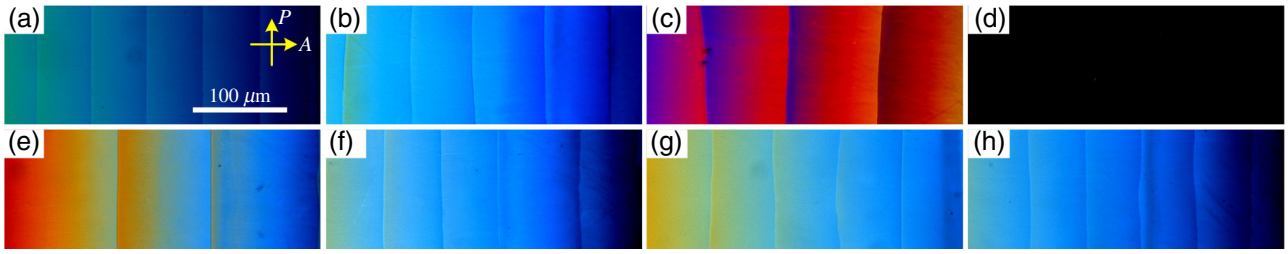

FIG. 3. Representative textures of the CLC system ($C_{M5} = 1.2\%$) in a wedged cell, at UV light intensities of (a) $I = 0$ mW cm^{-2}, (b) $I = 0.5$ mW cm^{-2}, (c) $I = 1.0$ mW cm^{-2}, (d) $I = 2.0$ mW cm^{-2}, (e) $I = 5.0$ mW cm^{-2}, (f) $I = 10.0$ mW cm^{-2}, (g) $I = 15.0$ mW cm^{-2}, and (h) $I = 20.0$ mW cm^{-2}. The shift of the disclination lines is due to the change of $P_0(I)$.

In order to track the change of P_0 under the effect of UV light and thus determine the relationship between P_0 and I for specific dopant concentrations of $C_{M5} = 0.8\%$ and $C_{M5} = 1.2\%$, the Grandjean-Cano method [1] is used. Wedge-shaped planar cells of 50 × 45 mm^2 size are prepared, where the thickness increased monotonically from zero to about 1 mm, corresponding to a wedge angle of $\alpha = 1.12°$. It allows the formation of regions with a different number of helical half turns of the director. The neighboring regions, characterized by consecutive numbers of helical half turns, are separated by disclination lines, as depicted by the POM snapshots in Figs. 3(a)–3(h) taken at crossed polarizers. The spacing L between two neighboring disclination lines is related to the natural pitch P_0 via the relation $|P_0| = 2\ L\ \tan\alpha$; in our case $\tan\alpha = 0.0196$. Upon increasing the UV intensity within the range $0 \le I \le I_c$, the spacing L between two neighboring disclination lines expanded gradually, as shown in Figs. 3(a)–3(c), indicating an increase of $|P_0|$, meanwhile keeping the initial (left) handedness. As $I \to I_c$, we found $L \to \infty$, which corresponds to the unwound state ($|P| = \infty$) and yields a total extinction of light [Fig. 3(d)]. At the further increase of I to $I > I_c$, the Grandjean texture reappeared, but with gradually shrinking L, as shown in Figs. 3(e)–3(h); it indicates a shortening of the pitch $|P_0|$, but with an opposite (right) handedness.

After removing the UV light, the CLCs returned to their original state [Fig. 3(a)] following the above sequence, just in reversed order.

The UV intensity dependence of the pitch $|P_0(I)|$, deduced from the above measurements, is plotted in Fig. 4(a). The effective HTP, $\beta_{M5}(I)$ of the dopant could also be calculated using Eq. (3) and is depicted in Fig. 4(b). Both figures demonstrate clearly the UV tunability of the helical pitch, as well as the UV-induced change of the handedness of the helix. The obtained behavior is in agreement with that reported recently for the other chiral antipode (M1) of the dopant [42].

Facilitating a comparison of measured data with the theoretical predictions, Fig. 4 depicts also the curves fitted to Eq. (8) of the model presented above. A good agreement is found at high intensities ($I > I_c$); at low intensities ($I < I_c$) only the trend is reproduced qualitatively. The fit parameters, $I_0 = 2.46 \pm 0.40$ mW cm^{-2} for $C_{M5} = 1.2\%$ and $I_0 = 2.10 \pm 0.25$ mW cm^{-2} for $C_{M5} = 0.8\%$, are above the relevant critical intensities I_c of the helix unwinding.

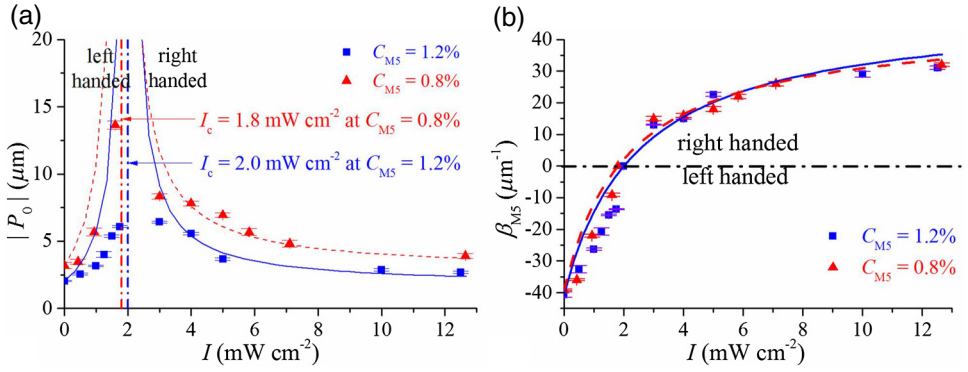

FIG. 4. (a) The pitch $|P_0|$ of the CLC systems ($C_{M5} = 0.8\%$ and $C_{M5} = 1.2\%$) and (b) the effective helical twisting power β_{M5} of the dopant M5 as a function of the UV intensity I. The symbols represent the measured data. Fits corresponding to Eq. (8) of the theoretical model are shown by the solid ($C_{M5} = 1.2\%$, $I_c = 2.0$ mW cm^{-2}, $I_0 = 2.46$ mW cm^{-2}) and dashed lines ($C_{M5} = 0.8\%$, $I_c = 1.8$ mW cm^{-2}, $I_0 = 2.10$ mW cm^{-2}). Dash-dotted lines indicate the critical intensities of the helix unwinding. Points of $|P_0| = 2000$ μm, measured near I_c are omitted from (a) for better appearance.

Taking into account Eq. (7) and the relation $X_s \leq 1$, it implies that $|\beta_M/\beta_P| > 1$, i.e., the unstable M5(M) conformer has higher HTP than the stable M5(P).

As seen in Fig. 4(a), at lower dopant concentration the pitch P_0 is always higher. Nevertheless, the $\beta_{M5}(I)$ relations obtained for the two concentrations are very close, as expected. The small difference detected in the critical intensities I_c (larger C_{M5} implies higher I_c) does not follow from the theoretical model presented. We attribute this deviation to the absorption of the light penetrating into the sample, which becomes stronger at higher dopant concentration.

IV. RESULTS AND DISCUSSION

The effects of light and ac electric field on the properties of CLCs as well as on the induced ECPs fall into four categories that are identified in our planar samples according to various combinations of light and the ac electric field:

(i) *equilibrium planar state* (PS_0) without light and electric field: here the CLC samples are unperturbed;
(ii) *EC state* (ECP_0) without light, but subjected to electric field: here the EC pattern is present;
(iii) *excited planar state* (PS_m) without electric field, but subjected to UV light: here various planar textures with a different number of half turns are observed;
(iv) *excited EC state* (ECP_m) subjected to a combination of UV light and electric field: here various EC patterns are seen.

Below we characterize these states in more detail.

A. The initial, equilibrium planar state

The initial, equilibrium planar state (PS_0) of the studied systems is obtained when the sample is not exposed to UV light ($I = 0$) and no voltage is applied. In contrast to the wedge cell used to determine $P_0(I)$ in Figs. 3 and 4, here the sample thickness is constant; thus we obtained a uniform planar texture with the number of half turns (k) being the same in the whole cell. The actual characteristics of the PS_0 state depend on the dopant concentration C_{M5}. Without dopant ($C_{M5} = 0$), we obtain the usual planar state of the host nematic (no helix, $k = 0$). Adding the dopant, the pitch $|P_0|$ decreases monotonically with increasing C_{M5}. Taking into account Eq. (3), this implies an increase of k in discrete steps. For example, for $C_{M5} = 0.2$, 0.6, and 1.2% we found $k = -1$, -3, and -6, respectively (the negative sign indicates the left handedness of the helix).

B. ECP driven by ac electric field only

For the host compound 1OO8 (pure NLC without chiral dopant), due to its negative dielectric anisotropy $\Delta\varepsilon = \varepsilon_{||} - \varepsilon_{\perp} < 0$, no uniform deformation (Freedericksz transition) can take place in a planar cell. Instead, the current-driven EC phenomenon can be observed, when the applied ac voltage U exceeded the U_{th} threshold value. The EC pattern (ECP_0) emerged from the initial PS_0 state at $U \geq U_{th}$ and manifested itself, in the used frequency range, as conductive normal rolls (Williams domains) with the rolls being perpendicular to the surface orientation $\mathbf{n}_0$; the periodicity of the rolls is about the cell thickness d [52].

Similarly, in our CLC samples composed of 1OO8 and the chiral dopant M5, the EC patterns (ECP_0) are detected in the form of conductive rolls; however, the orientation of rolls in ECP_0 is either parallel with or perpendicular to $\mathbf{n}_0$, depending on the concentration C_{M5} of the chiral dopant, as illustrated in Fig. 5. The concentration C_{M5} defines the number k of half turns of the helix in the PS_0 state, from which ECP_0 emerges. During this pattern formation, k does not change. It is thus plausible to attribute the changes in the roll direction to the variation of k with the concentration. Indeed, our observations justified this correlation: at concentrations where k is even, the rolls run normal to $\mathbf{n}_0$, while whenever k is odd, the rolls are parallel with $\mathbf{n}_0$.

It follows directly from the cell geometry that the director $\mathbf{n}_m$ in the middle of the cell depends on the parity of k. Whenever k is even, the director $\mathbf{n}_m$ in the middle of the cell is parallel with $\mathbf{n}_0$, while for odd k one has $\mathbf{n}_m \perp \mathbf{n}_0$. In view of this fact, we conclude that in the electroconvection of planar CLC systems, the EC rolls in ECP_0 should be

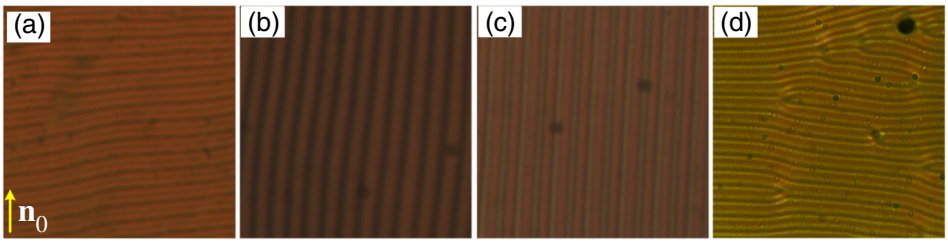

FIG. 5. Representative near-threshold ($U \geq U_{th}$) morphologies ($100 \times 100\ \mu m^2$) of ECPs without UV irradiation of CLCs at different C_{M5} dopant concentrations; $d = 6.0\ \mu m$, $f = 30$ Hz: (a) $U_{th} = 5.3$ V, $C_{M5} = 0.0\%$ and $\Lambda = 7.7\ \mu m$, $P = \infty$ ($k = 0$); (b) $U_{th} = 5.5$ V, $C_{M5} = 0.2\%$ and $\Lambda = 7.4\ \mu m$, $P = -12\ \mu m$ ($k = -1$); (c) $U_{th} = 5.8$ V, $C_{M5} = 0.6\%$ and $\Lambda = 7.4\ \mu m$, $P = -4\ \mu m$ ($k = -3$); (d) $U_{th} = 6.5$ V, $C_{M5} = 1.2\%$ and $\Lambda = 7.5\ \mu m$, $P = -2.05\ \mu m$ ($k = -6$).

perpendicular to the director $\mathbf{n}_m$ in the middle of the cell, rather than normal to the surface director $\mathbf{n}_0$. This conclusion is in agreement with previous observations [22] and simulation results [23] for small k ($|k| \leq 3$), as well as with findings in achiral twisted nematic samples ($k = 1/2$) [53].

We note that in our samples, the above-mentioned correlation between pattern orientation and $\mathbf{n}_m$ holds for $|k| > 3$ (at least up to $|k| = 6$) too, while previous studies reported rather the appearance of grid patterns for those larger k values [22,23]. Moreover, former simulations did not indicate a selectivity in the pattern direction for $|k| > 3$ (the free energy does not depend on the direction of the wave vector). Unfortunately, due to the lack of detailed parameter studies, it is unclear whether this different behavior can be accounted for simply by the difference in material parameters or whether there are other reasons.

Further inspection of the ECP_0 states presented in Fig. 5 indicates that the EC threshold U_{th} also depends on C_{M5}; a larger C_{M5} induces a higher U_{th}. As increasing C_{M5} means shorter $|P_0|$ and thus larger $|k|$, the growth of U_{th} agrees with the trend ($U \propto k^{1/2}$) predicted by the Helfrich-Hurault theory [18–20]. Interestingly, unlike the roll direction and U_{th}, the wavelength Λ of the rolls of ECP_0 is not sensitive to C_{M5} as confirmed by the data listed in the caption of Fig. 5.

C. Multiple planar states under UV illumination only

CLC systems unexposed to UV light are in the equilibrium planar state PS_0, where their pitch $P(I = 0)$ is determined by the dopant concentration C_{M5}. When illuminated with UV light, the natural pitch $|P_0(I)|$ varies with the intensity. Although the $|P_0(I)|$ dependence is continuous [though nonlinear and nonmonotonic according to Fig. 4(a)], as observed before in Sec. III, the actual pitch P can follow this variation in discrete steps only, jumping when the number k of the helical half turns is incremented (or decremented).

Indeed, we observe that upon increasing the UV intensity, in all CLC systems PS_0 transformed into a sequence of excited planar states (PS_m), which differ in their k value. Each transition between two neighboring planar states ($PS_m \rightarrow PS_{m+1}$), corresponds to incrementing or decrementing k by 1. For example, in the CLC with $C_{M5} = 1.2\%$, 12 transitions ($PS_0 \rightarrow PS_1 \rightarrow PS_2 \rightarrow \ldots \rightarrow PS_{11} \rightarrow PS_{12}$) can be identified, while the UV intensity reached the maximum value of $I = 20$ mW cm^{-2}. Figures 6(a)–6(e) show a few representatives (PS_0, PS_3, PS_6, PS_9, and PS_{12}, respectively) from the sequence of planar states.

The individual excited states can be distinguished in POM by their different extinction colors. The presence of colors indicates that in the studied CLC samples for $k \neq 0$, the Mauguin condition for adiabatic light propagation (the rotation of the light polarization together with the director) [1] is not fulfilled. Changing k alters the ellipticity of the transmitted elliptically polarized light and thus the extinction color too [54].

Each excited planar state PS_m possessed distinct UV intensity threshold I_m; hence a given PS_m with k half turns could exist if the illuminating intensity is in the range $I_m \leq I \leq I_{m+1}$; at the intensities limiting the range the natural pitches $P_0(I_m)$ and $P_0(I_{m+1})$ correspond to the limiting pitch values in Eq. (3). $P = P_0$ occurs only in the middle of the intensity range; at other intensities the helix is either compressed or dilated.

Inspection of the sequence of the PS_m states indicated that when the UV light intensity I is increased (but still remained within the $0 < I < I_c$ range), the induced $|P(I)|$ became larger and larger ($|P(I)| > |P(I = 0)|$); as an example, PS_3 is shown in Fig. 6(b); meanwhile, the CLC system still keeps the initial handedness (left-handed). Once I reaches the critical I_c, the resulting $|P_0(I_c)| = \infty$ made the system turn into the unwound state PS_6 (compensated cholesteric phase) without any helical structure ($|P(I_c)| = \infty$, $k = 0$), resulting in a dark image under crossed polarizers, as shown in Fig. 6(c). Actually, the

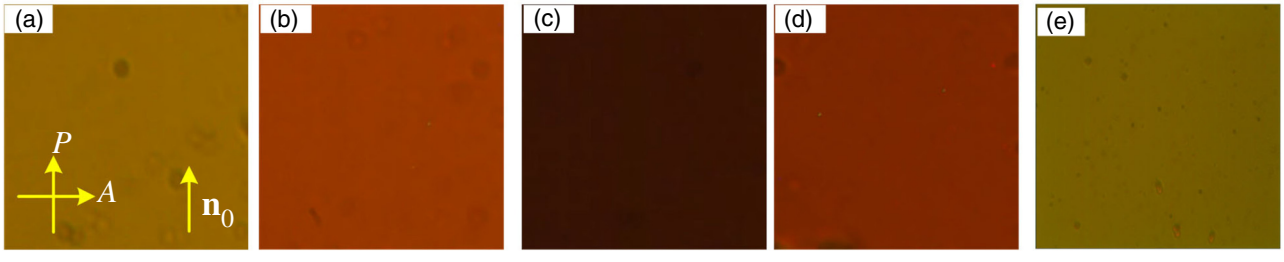

FIG. 6. Representative textures (100×100 μm^2) of planar states of CLCs ($C_{M5} = 1.2\%$) in a $d = 6.0$-μm-thick cell under UV light exposure with increasing I: (a) equilibrium planar state PS_0 with left-handed helix at $I = 0$ ($P \approx -2.05$ μm and $k = -6$); (b) planar state PS_3 with left-handed helix at $I = 1.25$ mW cm$^{-2} < I_c$ ($P = -4.0$ μm and $k = -3$); (c) compensated cholesteric state PS_6 at $I = I_c = 2.1$ mW cm^{-2} ($|P| = \infty$ and $k = 0$); (d) planar state PS_9 with right-handed helix at $I = 5.0$ mW cm$^{-2} > I_c$ ($P = 4.0$ μm and $k = 3$); (e) planar state PS_{12} with right-handed helix at $I = 20.0$ mW cm$^{-2} > I_c$ ($P = 2.05$ μm and $k = 3$).

unwound state is present not only for $I = I_c$, but also for the whole intensity range around it, where the condition $|P_0(I)| > 4\ d$, originating in Eq. (10) with $k = 0$, fulfils. Afterwards, if I is further enhanced, the system experienced a handedness inversion (from left-handed to right-handed), accompanied with decreasing $|P|$, as seen in PS_9 of Fig. 6(d). Finally, at very high I, P could even reach $P = -P(I = 0)$, as demonstrated in Fig. 6(e) by PS_{12}. Thus we conclude that $P(I)$ follows the $P_0(I)$ curve in a discretized, steplike manner.

When the UV light is turned off, the CLC systems go through the above states in reverse order ($PS_{12} \rightarrow PS_{11} \rightarrow \ldots \rightarrow PS_1 \rightarrow PS_0$), back to the initial equilibrium planar state PS_0.

D. The combined effect of light and ac electric field on the behavior of ECPs

When the sample is subjected to both UV illumination and an ac voltage exceeding U_{th}, various ECPs (ECP_m) are observed. The orientation of their convection rolls appeared either parallel with or perpendicular to $\mathbf{n}_0$, depending on the intensity of the UV light. The excited ECP_m states can be reached along two routes. First, starting from the UV excited PS_m planar state, upon increasing the voltage above U_{th} ECP_m emerges, which relaxes back to the PS_m state when the voltage is switched off. Second, starting from the ECP_0 state (without UV), increasing the UV intensity a sequential transition through the excited EC states ($ECP_0 \rightarrow ECP_1 \rightarrow ECP_2 \rightarrow \ldots$) can be found. For example, in the CLC with $C_{M5} = 1.2\%$, whose few excited PS_m planar states are shown in Fig. 6, 12e transitions ($ECP_0 \rightarrow ECP_1 \rightarrow \ldots \rightarrow ECP_{11} \rightarrow ECP_{12}$) are detected upon increasing the UV intensity to the maximum value of $I = 20\ \mathrm{mW\,cm^{-2}}$. Figures 7(a)–7(e) show some representatives (ECP_0, ECP_3, ECP_6, ECP_9, and ECP_{12}, respectively) of the sequence. Each ECP_m state relaxed to the corresponding planar state PS_m after cancellation of the ac field.

The various *excited EC states* ECP_m can be selected by different I, i.e., each ECP_m exists in its own UV intensity range $I_m \leq I \leq I_{m+1}$, coinciding with that of the corresponding *excited planar state* PS_m mentioned above. The strong correlation between the PS_m and ECP_m states implies that both has the same number k of half turns. The photoswitching between ECPs at increasing or decreasing I is reversible, with the timescale of seconds.

Section IV B discusses the consequences of varying the dopant concentration on ECP_0. Under those conditions, the direction of EC rolls depends on the director $\mathbf{n}_m$ in the middle of the cell, which in turn is governed by the number k of half turns. It should be irrelevant whether a change in P is caused by altering the dopant concentration or by the UV illumination (as in Sec. IV C). Thus, it is anticipated that the orientation of the rolls in ECPs should be switchable between being normal to and parallel with $\mathbf{n}_0$ (in both cases normal to $\mathbf{n}_m$), simply by selecting proper UV light intensities (and by that the appropriate k). The observations presented in Fig. 7, and in the forthcoming Figs. 9 and 10 are in full agreement with the above conclusion.

In contrast to the direction of the wave vector of the pattern, its magnitude and hence the spatial periodicity Λ of the ECPs are not affected by the UV intensity, i.e., by the variation of the pitch. The independence of Λ on P is already seen in Fig. 5, where the changes of P are induced by different C_{M5} concentrations. This behavior does not match the theoretical expectations, which anticipate $\Lambda \propto (d\,P)^{1/2}$ [20,22,25].

Further inspection of the ECP_m sequences implied that the threshold voltage U_{th} is also affected by the UV illumination, as presented in Fig. 8. Comparing the $U_{th}(I)$ curve with the $|P_0(I)|$ curve shown in Fig. 4(a), we deduce that the threshold voltage is lowest in the compensated cholesteric (PS_6) state where $|P| = \infty$ and thus $k = 0$.

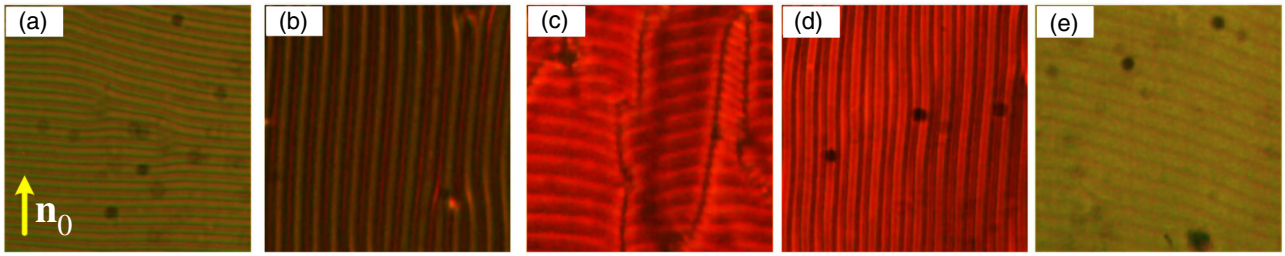

FIG. 7. Representative morphologies ($100 \times 100\ \mu m^2$) of ECPs in CLC ($C_{M5} = 1.2\%$) upon illumination with UV light of different I: (a) ECP_0 in a left-handed CLC at $I = 0$ ($P = -2.05\ \mu m$), $U_{th} = 6.5$ V, $\Lambda = 7.2\ \mu m$ and $k = -6$; (b) ECP_3 in a left-handed CLC at $I = 1.25\ \mathrm{mW\,cm^{-2}} < I_c$ ($P = -4.0\ \mu m$), $U_{th} = 4.6$ V, $\Lambda = 7.7\ \mu m$ and $k = -3$; (c) ECP_6 in the compensated cholesteric state at $I = I_c = 2.09\ \mathrm{mW\,cm^{-2}}$ ($|P| = \infty$), $U_{th} = 4.2$ V, $\Lambda = 7.2\ \mu m$ and $k = 0$; (d) ECP_9 in a right-handed CLC at $I = 5.0\ \mathrm{mW\,cm^{-2}} > I_c$ ($P = 4.0\ \mu m$), $U_{th} = 4.7$ V, $\Lambda = 8.3\ \mu m$ and $k = 3$; (e) ECP_{12} in a right-handed CLC at $I = 20.0\ \mathrm{mW\,cm^{-2}} > I_c$ ($P = 2.05\ \mu m$), $U_{th} = 6.6$ V, $\Lambda = 7.2\ \mu m$ and $k = 6$.

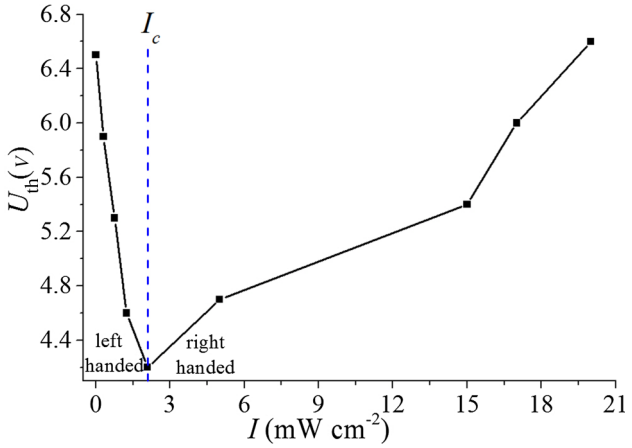

FIG. 8. Dependence of U_{th} on the UV intensity I for the CLC with $C_{M5} = 1.2\%$. The left-hand side of the curve corresponds to the case where $|P|$ increased with enhanced I in a left-handed CLC system, whereas the right-hand side of the curve corresponds to the case where $|P|$ decreased with enhanced I in a right-handed CLC system. The turning point at I_c (marked by the dashed line) corresponds to the case of compensated cholesteric with $|P| = \infty$ ($k = 0$).

Decreasing $|P|$, i.e., increasing $|k|$ results in higher threshold voltages. Tuning P_0 with the dopant concentration in Sec. IV B yields similar results. These observations are in accordance with the trend $U \propto |k|^{1/2}$ provided by the Helfrich-Hurault model [18–20]. We note, however, that improvements of this model [23–25,27] inspired by former experimental data [21–26] points out the importance of helix compression or dilation (i.e., the effect of $P \neq P_0$), which yields nonmonotonic $U_{th}(d/P_0)$ dependence in wedge-shaped cells. As under our experimental conditions (planar cell with UV-intensity-dependent pitch) the helix changes from compressed to dilated, when the UV intensity sweeps through the intensity range of existence ($I_m \leq I \leq I_{m+1}$) of a PS_m (or ECP_m) state, the same mechanism is expected to be effective. Thus $U_{th}(I)$ is anticipated to be a sawtoothlike function with jumps at the intensity values, where k changes. Justification of this prediction (which requires measurements with much higher intensity resolution), however, falls outside the scope of the present paper; nevertheless, it is an interesting problem that may be the subject of a future project.

E. Photodynamic characteristics of the transitions between EC patterns

In the previous sections, the steady-state behavior of the ECPs is discussed. In contrast, if the UV intensity is changed suddenly, a photoswitching between two ECP states can be detected. In general, it is found that photoswitching is reversible, occurring on a time scale of seconds; a transition induced by increasing I can be reversed by the reduction of I. The experimental studies of the details of the photoswitching process are constrained to low UV intensities, to the transitions between the ECP_0 (unexposed) and the ECP_1 (illuminated) states of the CLC with $C_{M5} = 1.2\%$.

1. The effect of UV light on the transition process

Two kinds of dynamic transitions should be distinguished. The transition occurring upon illumination by UV light we call ON transitions, while for that induced by switching off the illumination, we use the term OFF transition. Note that an ac voltage is continuously applied during both kinds of transitions.

The time evolution of the patterns during the ON and OFF transition processes is demonstrated in Figs. 9 and 10, respectively, for the case of low ($I = 0.7$ mW cm^{-2}) UV intensity, where illumination causes only a change of k by 1. The two ECP states, ECP_0 (with $k = -6$) and ECP_1 (with $k = -5$), can be distinguished by the different direction of the EC rolls as well as by the different extinction color of their background. Apparently, the photoswitching between these states is not jumplike; instead, it is a gradual process. As seen in Fig. 9, during the $ECP_0 \rightarrow ECP_1$ (ON) transition, first the initial ECP_0 state [Fig. 9(a)] undergoes a slow decay [Figs. 9(b) and 9(c)], then the final

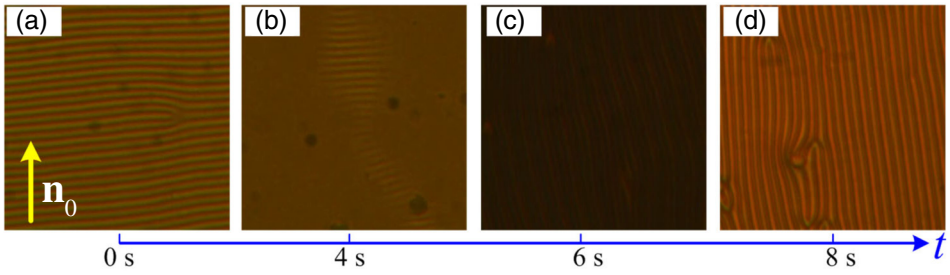

FIG. 9. Temporal evolution of ECPs (100×100 μm^2) at a fixed ac field ($U = 6.5$ V) during illumination with a weak UV light ($I = 0.7$ mW cm^{-2}), corresponding to an ON transition process between two neighboring ECPs ($C_{M5} = 1.2\%$): (a) the initial ECP_0 under ac field (without UV exposure); (b),(c) intermediate states under ac field and UV light; (d) the final ECP_1 under ac field and UV light.

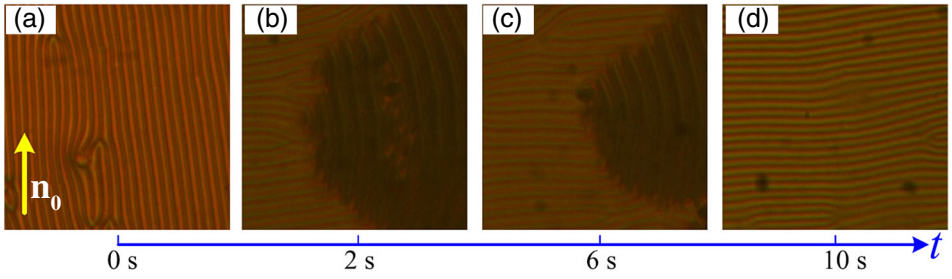

FIG. 10. Temporal evolution of ECPs (100×100 μm^2) following the switch off of the UV light while holding a fixed ac field ($U = 6.5$ V), representative of the OFF transition process between two neighboring ECPs ($C_{M5} = 1.2\%$): (a) ECP_1 under ac field and UV light; (b),(c) intermediate states under ac field (without UV exposure); (d) ECP_0 under ac field (without UV exposure).

ECP_1 state emerges, experiences a growth, and finally takes over in the whole sample finishing the transition [Fig. 9(d)]. Similarly, during the $ECP_1 \rightarrow ECP_0$ (OFF) transition following the turning off of the UV illumination, in the ECP_1 pattern [Fig. 10(a)], domains of ECP_0 nucleate [Figs. 10(b) and 10(c)], which grow to fill the sample finally [Fig. 10(d)]. Both the ON and the OFF processes require several seconds to terminate.

From the above description it is clear that the photoswitching between two patterned states is a complex phenomenon that, in contrast to the electro-optical switching of LCDs, cannot be characterized by a single relaxation time. This complexity is illustrated in Figs. 11(a) and 11(b), which depict the temporal evolution of the light intensities diffracted by the ECP_0 and ECP_1 states during the ON and the OFF transitions, respectively. These intensities are measured simultaneously by two photodetectors placed at the proper diffraction angles. The oscillation of the diffraction intensity is a property of the stationary state of electroconvection, where the director tilt has a modulation with double the driving frequency of the ac electric field. This intensity modulation is suppressed during the switching transient, but recovers with the stabilization of the distortion and convection in the new stationary ECP state. The diffraction dynamics (formation and decay) of ECP_0 and ECP_1 is in coincidence with the morphological changes shown in Figs. 9 and 10.

2. Effect of ac voltage on the transition process

Interestingly, the transition processes can be affected by changing the ac voltage U. This is demonstrated for the $ECP_0 \rightarrow ECP_1$ (ON) transition in Fig. 12. Figure 12(a) shows the same ECP_0 state as in Fig. 9(a), where only an ac voltage of $U \approx U_{0th} = 6.5$ V is applied. For a few seconds after switching on the UV light, at the stages of Figs. 12(b) and 12(c), both UV light and the ac voltage $U \approx 6.5$ V have been on; finally, at the stage of Fig. 12(d), keeping UV still on, U is increased to exceed another threshold $U_{0th\_ON} = 7.0$ V. Surprisingly, instead of obtaining the expected final ECP_1 state [Fig. 9(d)], the initial ECP_0 recovers even in the presence of UV light [Fig. 12(d)]. Note that neither the direction of the rolls, nor the extinction color of the background changes, indicating that k is unaltered.

For the $ECP_1 \rightarrow ECP_0$ (OFF) transition depicted in Fig. 13, we start from ECP_1, where both UV light and ac voltage are applied. It should be noted, however, that the voltage in Fig. 13(a), $U \approx U_{1th} = 5.3$ V, is lower than that in Fig. 10(d), since, in accordance with Fig. 8, the threshold U_{1th} of ECP_1 is lower than the threshold U_{0th} of ECP_0. Then, at the stages of Figs. 13(b) and 13(c), the UV illumination is cancelled, while the ac voltage remains unchanged. As a result ECP_1 disappears gradually, relaxing back toward the equilibrium planar state PS_0. However, if at that point [after Fig. 13(c)], U is

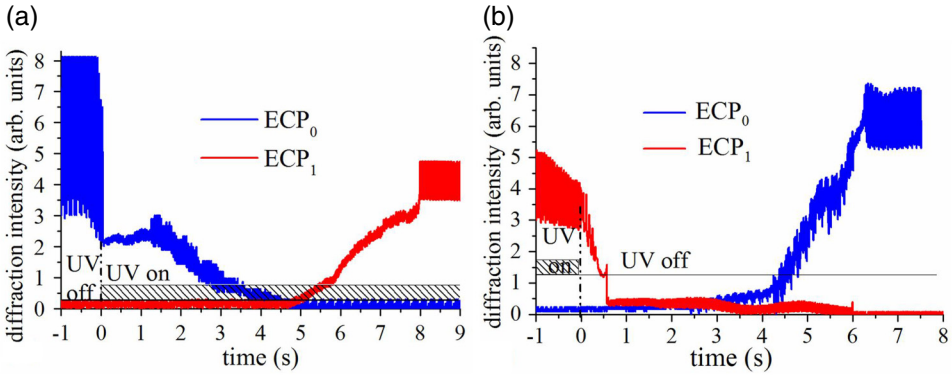

FIG. 11. Temporal evolution of the diffraction intensities of ECP_0 and ECP_1 following (a) switching on a weak ($I = 0.7$ mW cm^{-2}) UV light representing an ON transition, (b) switching off the UV light corresponding to an OFF transition. A fixed ac field ($U = 6.5$ V) is held continuously; $C_{M5} = 1.2\%$.

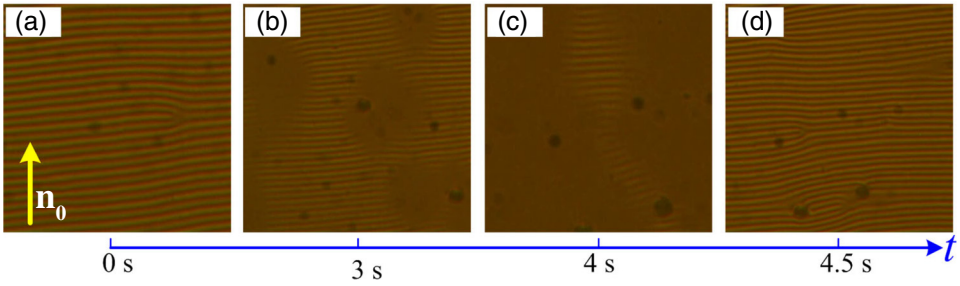

FIG. 12. Effect of an increased ac voltage on the ON transition process. (a) The initial ECP_0 driven by $U \approx U_{0th}$ only; (b) ECP_0 becomes fuzzy under UV illumination ($I = 0.7$ mW cm^{-2}); (c) then ECP_0 almost disappears with time; (d) however, with the increased $U = U_{0th_{ON}} = 7.0\,\text{V} > U_{0th} = 6.5\,\text{V}$, the initial ECP_0 reappears.

increased over another threshold $U_{1thOFF} = 5.6$ V, still without being exposed to UV, instead of the expected relaxation to PS_0, the pattern ECP_1 reappears [Fig. 13(d)]. Again, neither the direction of the rolls, nor the extinction color of the background changed, i.e., k remains unchanged.

Normally, during photoswitching between neighboring EC states ($ECP_0 \leftrightarrow ECP_1$, Figs. 9 and 10) induced by the sudden alteration of the UV intensity, k has to change. Figures 12 and 13, however, demonstrate that this photoswitching can be blocked by applying appropriate voltages, when neither pattern rotation nor background color change occurs. These findings prove that in those cases k does not change, even though it should happen due to the modification of the UV intensity. This is highly surprising, especially in view of the fact that the dielectric contribution to the free energy of the system is independent of the number of half turns. The reason why a high enough voltage can freeze the system in an energetically unfavored, metastable state is yet unclear. A possible cause may lie in the mechanism of the change of k. A homogeneous planar sample (ideally) has no thickness gradients; therefore, it has no Grandjean disclinations separating domains with different k values. In such samples, unlike in wedge cells, the jump in k is not a smooth elastic deformation; it requires first a nucleation of a disclination loop around the germ of a new domain (new k), then its spreading over the sample. As a possible clue, one may assume that at the process of nucleation the director may need to gain n_z components (otherwise not present in the PS_m states), which may become harder under higher voltages due to the negative dielectric anisotropy.

V. CONCLUSION

Systematic investigations of a CLC containing a photoresponsive chiral dye explored that illumination by UV light leads to the occurrence of multiple electroconvection patterns and allows photoswitching between them. These phenomena are due to the UV light-induced change of the pitch (including handedness inversion), which forces the change of the helical half turns in the sample and makes the wave vector as well as the AC threshold voltage of the EC patterns tunable by the intensity of the UV light.

The possibility of convenient and remote manipulation of the light intensity allows the tuning of ECPs, which can potentially be exploited in designing certain photonic devices, such as controllable gratings, to implement dual-mode operations *in situ* and online. We hope our pioneering work on this light tunability will start an alternative branch of application of EC patterns.

ACKNOWLEDGMENTS

Illuminating discussion with I. Jánossy is gratefully acknowledged. We thank H. Yang from Peking University for providing M5. Á.B. is grateful for the hospitality of The Grant of 2017 Guangdong Recruitment Program of Foreign Experts by Guangdong Foreign Experts Administration.

This work is supported by the National Natural Science Foundation of China (Grant Nos. 11374067 and 11774070), the Guangdong Provincial Science and Technology Plan (Grant Nos. 2014A050503064, 2016A050502055, and 2017A030313036), and the National Research, Development and Innovation Office (NKFIH) (Grant No. FK 125134).

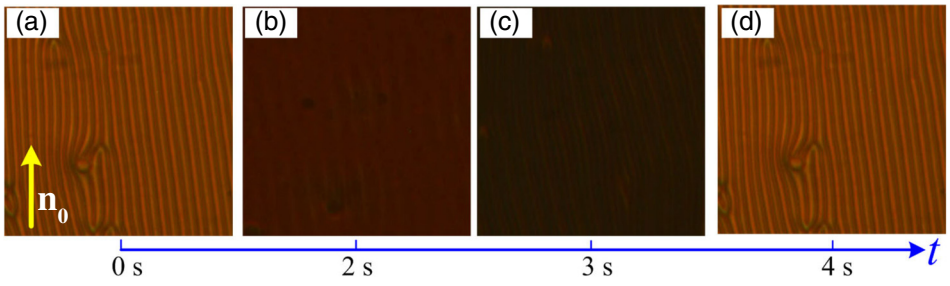

FIG. 13. Effect of ac voltage on the OFF transition process. (a) ECP_1 under UV ($I = 0.7$ mW cm^2) and ac fields; (b),(c) UV light is off, while the ac field is still on, ECP_1 disappears gradually with time; (d) however, with an increased voltage $U = U_{1thOFF} = 5.6\,\text{V} > U_{1th} = 5.3\,\text{V}$, the ECP_1 state is revived.

[1] P. G. de Gennes and J. Prost, *The Physics of Liquid Crystals*, 2nd ed. (Clarendon Press, Oxford, 1993).

[2] W. Lee and S. T. Wu, Focus issue introduction: Liquid crystal materials for photonic applications, Opt. Mater. Express **1**, 1585 (2011).

[3] J. Kim, J. H. Suh, B. Y. Lee, S. U. Kim, and S. D. Lee, Optically switchable grating based on dye-doped ferroelectric liquid crystal with high efficiency, Opt. Express **23**, 12619 (2015).

[4] Y. Xiang, H. Z. Jing, Z. D. Zhang, W. J. Ye, M. Y. Xu, E. Wang, P. Salamon, N. Éber, and A. Buka, Tunable Optical Grating Based on the Flexoelectric Effect in a Bent-Core Nematic Liquid Crystal, Phys. Rev. Appl. **7**, 064032 (2017).

[5] H. Z. Jing, Y. Xiang, M. Y. Xu, Z. D. Zhang, Z. D. Cheng, D. Shen, Z. G. Zheng, J. L. Li, M. J Zhou, E. Wang, Y. Q. Wang, and Y. H. Cai, Polarity-dependent bistable optical grating in chiral bent-core nematic liquid crystals, Opt. Mater. Express **6**, 2584 (2016).

[6] L. Kramer and W. Pesch, in *Pattern Formation in Liquid Crystals*, edited by A. Buka and L. Kramer (Springer, Berlin, 1996), pp. 221–255.

[7] A. Buka, N. Eber, W. Pesch, and L. Kramer, in *Self Assembly, Pattern Formation and Growth Phenomena in Nano-Systems*, edited by A. A. Golovin and A. A. Nepomnyashchy (Springer, Dordrecht, 2006), pp. 55–82.

[8] N. Éber, P. Salamon, and Á. Buka, Electrically induced patterns in nematics and how to avoid them, Liq. Cryst. Rev. **4**, 101 (2016).

[9] A. Buka, N. Eber, W. Pesch, and L. Kramer, Isotropic and anisotropic electroconvection, Phys. Rep. **448**, 115 (2007).

[10] W. Helfrich, Conduction-induced alignment of nematic liquid crystals: Basic model and stability considerations, J. Chem. Phys. **51**, 4092 (1969).

[11] M. de Zwart, Distortion of the cholesteric planar texture in liquid crystals with a negative dielectric anisotropy, J. Phys. (Paris) **39**, 423 (1978).

[12] F. Rondelez, H. Arnould, and G. J. Gerritsma, Electrohydrodynamic Effects in Cholesteric Liquid Crystals under AC Electric Fields, Phys. Rev. Lett. **28**, 735 (1972).

[13] H. Arnould-Netillard and F. Rondelez, Electrohydrodynamic instabilities in cholesteric liquid crystals with negative dielectric anisotropy, Mol. Cryst. Liq. Cryst. **26**, 11 (1974).

[14] T. Kohno, H. Miike, and Y. Ebina, The instability of planar texture in cholesteric and nematic mixture with the negative dielectric anisotropy, J. Phys. Soc. Jpn. **44**, 1678 (1978).

[15] J. H. Huh, Y. Akasako, and S. Kai, New characteristics of electrohydrodynamic instability in a nematic liquid crystal doped with a cholesteric one, J. Phys. Soc. Jpn. **73**, 2975 (2004).

[16] C. J. Gerritsma and P. van Zanten, Periodic perturbations in the cholesteric plane texture, Phys. Lett. A **37**, 47 (1971).

[17] F. Rondelez and H. Arnould, Déformations de la texture planaire d'un cholestérique á grand pas sous l'action d'un champ électrique, C. R. Acad. Sci. B **273**, 549 (1971).

[18] W. Helfrich, Electrohydrodynamic and dielectric instabilities of cholesteric liquid crystals, J. Chem. Phys. **55**, 839 (1971).

[19] H. Hervet, J. P. Hurault, and F. Rondelez, Static one-dimensional distortions in cholesteric liquid crystals, Phys. Rev. A **8**, 3055 (1973).

[20] J. P. Hurault, Static distortions of a cholesteric planar structure induced by magnetic or AC electric fields, J. Chem. Phys. **59**, 2068 (1973).

[21] T. J. Scheffer, Electric and Magnetic Field Investigations of the Periodic Gridlike Deformation of a Cholesteric Liquid Crystal, Phys. Rev. Lett. **28**, 593 (1972).

[22] S. V. Belyaev and L. M. Blinov, Instability of planar texture of a cholesteric liquid crystal in an electric field, Sov. Phys. JETP **43**, 96 (1976).

[23] V. G. Chigrinov, V. V. Belyaev, S. V. Belyaev, and M. F. Grebenkin, Instability of cholesteric liquid crystals in an electric field, Sov. Phys. JETP **50**, 994 (1979).

[24] M. de Zwart and C. Z. van Doorn, The field-induced square grid perturbation in the planar texture of cholesteric liquid crystal, J. Phys. (Paris) Coll. **44**, C3-278 (1979).

[25] N. Éber and I. Jánossy, Thickness dependence of threshold field for instabilities in cholesterics, Mol. Cryst. Liq. Cryst. **49**, 137 (1979).

[26] S. Hirata, I. Matsuzaki, A. Yanagita, and T. Tako, Successive transitions in cholesteric liquid crystals, J. Phys. Soc. Jpn. **50**, 3862 (1981).

[27] G. Vertogen and E. W. C. van Groesen, The field-induced instability in the planar texture of cholesteric liquid crystals, J. Chem. Phys. **76**, 2043 (1982).

[28] W. Hu, H. Zhao, L. Song, Z. Yang, H. Cao, Z. Cheng, Q. Liu, and H. Yang, Electrically controllable selective reflection of chiral nematic liquid crystal/chiral ionic liquid composites, Adv. Mater. **22**, 468 (2010).

[29] X. Chen, L. Wang, Y. Chen, C. Li, G. Hou, X. Liu, X. Zhang, W. He, and H. Yang, Broadband reflection of polymer-stabilized chiral nematic liquid crystals induced by a chiral azobenzene compound, Chem. Commun. **50**, 691 (2014).

[30] L. Zhang, M. Wang, L. Wang, D.-K. Yang, H. Yu, and H. Yang, Polymeric infrared reflective thin films with ultra-broad bandwidth, Liq. Cryst. **43**, 750 (2016).

[31] J. Geng, C. Dong, L. Zhang, Z. Ma, L. Shi, H. Cao, and H. Yang, Electrically addressed and thermally erased cholesteric cells, Appl. Phys. Lett. **89**, 081130 (2006).

[32] T. Nose, T. Miyanishi, Y. Aizawa, R. Ito, and M. Honma, Rotational behavior of stripe domains appearing in hybrid aligned chiral nematic liquid crystal cells, Jpn. J. Appl. Phys. **49**, 311 (2010).

[33] C. H. Lin, R. H. Chiang, S. H. Liu, C. T. Kuo, and C. Y. Huang, Rotatable diffractive gratings based on hybrid-aligned cholesteric liquid crystals, Opt. Express **20**, 26837 (2012).

[34] L. Zhang, L. Wang, U. S. Hiremath, H. K. Bisoyi, G. G. Nair, C. V. Yelamaggad, A. M. Urbas, T. J. Bunning, and Q. Li, Dynamic orthogonal switching of a thermoresponsive self-organized helical superstructure, Adv. Mater. **29**, 1700676 (2017).

[35] A. Y. G. Fuh, C. H. Lin, and C. Y. Huang, Dynamic pattern formation and beam-steering characteristics of cholesteric gratings, Jpn. J. Appl. Phys. **41**(Part 1, No. 1), 211 (2002).

[36] M. Czajkowski, J. Klajn, J. Cybińska, J. Feder-Kubis, and K. Komorowska, Cholesteric gratings induced by electric field in mixtures of liquid crystal and novel chiral ionic liquid, Liq. Cryst. **44**, 911 (2016).

[37] Z. Zheng, B. Liu, L. Zhou, W. Wang, W. Hu, and D. Shen, Wide tunable lasing in photoresponsive chiral liquid crystal emulsion, J. Mater. Chem. C **3**, 2462 (2015).

[38] J. B. Guo, H. Wu, F. J. Chen, L. P. Zhang, W. L. He, H. Yang, and J. Wei, Fabrication of multi-pitched photonic structure in cholesteric liquid crystals based on a polymer template with helical structure, J. Mater. Chem. C **20**, 4094 (2010).

[39] H. C. Jau, T. H. Lin, Y. Y. Chen, C. W. Chen, J. H. Liu, and Andy Y. G. Fuh, Direction switching and beam steering of cholesteric liquid crystal gratings, Appl. Phys. Lett. **100**, 131909 (2012).

[40] P. Z. Sun, Z. Liu, W. Wang, L. L. Ma, D. Shen, W. Hu, Y. Q. Lu, L. J. Chen, and Z. G. Zheng, Light-reconfigured waveband-selective diffraction device enabled by micropatterning of a photoresponsive self-organized helical superstructure, J. Mater. Chem. C **4**, 9325 (2016).

[41] H. C. Jau, T. H. Lin, R. X. Fung, S. Y. Huang, J. H. Liu, and Andy Y. G. Fuh, Optically-tunable beam steering grating based on azobenzene doped cholesteric liquid crystal, Opt. Express.**18**,17498 (2010).

[42] J. Sun, L. Yu, L. Wang, C. Li, Z. Yang, W. He, C. Zhang, L. Zhang, J. Xiao, X. Yuan, F. Lie, and H. Yang, Optical intensity-driven reversible photonic bandgaps in self-organized helical superstructures with handedness inversion, J. Mater. Chem. C **5**, 3678 (2017).

[43] Z. Zheng, Y. Li, H. K. Bisoyi, L. Wang, T. J. Bunning, and Q. Li, Three-dimensional control of the helical axis of a chiral nematic liquid crystal by light, Nature **531**, 352 (2016).

[44] J. Sun, R. Lan, Y. Gao, M. Wang, W. Zhang, L. Wang, L. Zhang, Z. Yang, and H. Yang, Stimuli-directed dynamic reconfiguration in self-organized helical superstructures enabled by chemical kinetics of chiral molecular motors, Adv. Sci. **5**, 1700613 (2017).

[45] I. Gvozdovskyy, O. Yaroshchuk, M. Serbina, and R. Yamaguchi, Photoinduced helical inversion in cholesteric liquid crystal cells with homeotropic anchoring, Opt. Express **20**, 3499 (2012).

[46] A. Ryabchun, A. Bobrovsky, J. Stumpe, and V. Shibaev, Rotatable diffraction gratings based on cholesteric liquid crystals with phototunable helix pitch, Adv. Opt. Mater. **3**, 1273 (2015).

[47] Y. Xiang, Y. K. Liu, A. Buka, N. Éber, Z. Y. Zhang, M. Y. Xu, and E. Wang, Electric-field-induced patterns and their temperature dependence in a bent-core liquid crystal, Phys. Rev. E **89**, 012502 (2014).

[48] Y. Xiang, J. W. Goodby, V. Görtz, and H. F. Gleeson, Revealing the uniaxial to biaxial nematic liquid crystal phase transition via distinctive electroconvection, Appl. Phys. Lett. **94**, 145506 (2009).

[49] Y. Xiang, M. J. Zhou, M. Y. Xu, P. Salamon, N. Éber, and Á. Buka, Unusual polarity-dependent patterns in a bent-core nematic liquid crystal under low-frequency AC field, Phys. Rev. E **91**, 042501 (2015).

[50] J. P. van Meter and B. H. Klanderman, Mesomorphic properties of some phenyl benzoate derivatives, Mol. Cryst. Liq. Cryst. **22**, 271 (1973).

[51] D. Statman and I. Jánossy, Study of photoisomerization of azo dyes in liquid crystals, J. Chem. Phys. **118**, 3222 (2003).

[52] N. Eber, L. O. Palomares, P. Salamon, A. Krekhov, and A. Buka, Temporal evolution and alternation of mechanisms of electric-field-induced patterns at ultralow-frequency driving, Phys. Rev. E **86**, 021702 (2012).

[53] H. Bohatsch and R. Stannarius, Frequency-induced structure transition of nematic electroconvection in twist cells, Phys. Rev. E **60**(5 Pt A), 5591 (1999).

[54] I. Jánossy, T. Tóth-Katona, T. Kósa, and L. Sukhomlinova, Super-twist generation and instabilities in photosensitive liquid crystal cells, J. Mol. Liq. (2018).